ENVIRONMENTAL RESEARCH
LETTERS

LETTER • OPEN ACCESS

The North Pacific Blob acts to increase the predictability of the Atlantic warm pool

ENVIRONMENTAL RESEARCH
LETTERS

OPEN ACCESS

RECEIVED
10 February 2021

REVISED
24 April 2021

ACCEPTED FOR PUBLICATION
11 May 2021

PUBLISHED
25 May 2021

LETTER

The North Pacific Blob acts to increase the predictability of the Atlantic warm pool

Yusen Liu[1], Cheng Sun[1,*], Fred Kucharski[2,3], Jianping Li[4,5], Chunzai Wang[6] and Ruiqiang Ding[7]

[1] College of Global Change and Earth System Science (GCESS), Beijing Normal University, Beijing, People's Republic of China
[2] The Abdus Salam International Centre for Theoretical Physics, Trieste, Italy
[3] Center of Excellence for Climate Change Research/Department of Meteorology, King Abdulaziz University, Jeddah, Saudi Arabia
[4] Frontiers Science Center for Deep Ocean Multispheres and Earth System (FDOMES)/Key Laboratory of Physical Oceanography/Institute for Advanced Ocean Studies, Ocean University of China, Qingdao 266100, People's Republic of China
[5] Laboratory for Ocean Dynamics and Climate, Pilot Qingdao National Laboratory for Marine Science and Technology, Qingdao 266237, People's Republic of China
[6] State Key Laboratory of Tropical Oceanography (LTO), South China Sea Institute of Oceanology, Chinese Academy of Sciences, Guangzhou, People's Republic of China
[7] State Key Laboratory of Earth Surface Processes and Resource Ecology, Beijing Normal University, Beijing 100875, People's Republic of China
[*] Author to whom any correspondence should be addressed.

E-mail: scheng@bnu.edu.cn

Keywords: Atlantic warm pool, North Pacific blob, inter-basin teleconnection, marine heatwave, warm pool prediction

Supplementary material for this article is available online

Abstract

The Atlantic warm pool (AWP) has profound impacts on extreme weather events and climate variability. Factors influencing the AWP and its predictability are still not fully understood. Other than local ocean–atmosphere feedbacks and El Niño Southern Oscillation, we find an extratropical precursor from the Northeast Pacific (known as the Blob), which leads the AWP by 1 year with a robust correlation ($r = 0.68$). A suite of Northeast Pacific pacemaker experiments successfully reproduces the leading influence of the Blob on the AWP. The preceding summer Blob-related sea surface temperature (SST) warming signal can be transmitted towards the lower latitudes through the seasonal footprint mechanism, leading to the central Pacific warming in the winter and following spring. Such a strong tropical Pacific SST heating excites an anomalous atmospheric wave train that resembles the Pacific/North American (PNA) teleconnection pattern. At the downstream portion of the PNA, the low sea surface pressure anomalies can be found over the AWP region during the following spring. The anomalous low initiates the AWP SST warming, and the AWP warmer SST can persist into summer and is further amplified due to ocean–atmosphere feedbacks. Our results show that the North Pacific Blob may act as a useful predictor of the AWP 1 year in advance through trans-basin interactions. A Blob-based prediction model shows considerable hindcast skill for the observed AWP SST anomaly.

1. Introduction

The Atlantic warm pool (AWP) is a part of the Western Hemisphere warm pool (WHWP), which is also the second-largest warm pool in the world. The AWP is undoubtedly influential to the overlying atmosphere regionally or remotely. The impacts of the AWP on weather patterns and global climate have received considerable attention. For instance, the AWP contributes a lot to the moisture transport in North America and can even reach Western Europe during the summer when it is the largest in size [1–5]. The AWP is also capable of inducing changes from local circulation (e.g. sea breezes) [6] to large-scale systems like the North Atlantic subtropical high and Caribbean low-level jet at an annual scale, resulting in the changes in precipitation over the surrounding regions [7–9]. In addition, the influences of the AWP on hurricanes are significant. The vertical wind shear is reduced in response to the sea surface temperature (SST) warming, therefore increasing the instability of the troposphere and energizing deep convections,

which are favorable for the formation and development of hurricanes [9–11]. Moreover, a previous study also suggested that the AWP plays an intermedia role in linking the Atlantic multidecadal oscillation and hurricanes [12]. Given the implications that the impacts of the AWP may not be limited in the Atlantic basin, a recent study has found the AWP as a precursor of El Niño Southern Oscillation (ENSO) for 1 year ahead [13]. Also, anomalous SST warming induced by the AWP excites a westward propagation of the Rossby wave that changes the meridional circulation over the western North Pacific, modulating the climate variability (next winter) through local air–sea interaction [14]. It is suggested that the AWP plays a role in the Atlantic–Pacific trans-basin teleconnections [15, 16].

Several mechanisms have been proposed to understand the variability of the AWP. Some studies pointed out that the SST evolution of the AWP partly relies on the local air–sea feedbacks associated with net heat fluxes [17]. For instance, the weakened northeast trade winds reduce latent heat fluxes through less evaporation and consequently leads to SST warming [18, 19]. At interannual time scales, ENSO is one of the most prominent climate signals in the world [20]. It is suggested that El Niño can induce strong SST warming over the tropical North Atlantic as well as the AWP [21–23]. The mature phase of ENSO in the preceding winter leads to a large warm pool during the spring and early summer [24]. The ENSO-induced large-scale circulation changes, like weakened trade winds and subtropical subsidence, provide favorable backgrounds for local air–sea feedback to develop, together contribute to the evolution of the AWP. However, based on a case study, the occurrence of ENSO does not always guarantee a stronger AWP [25], suggesting that considerable uncertainties still exist in predicting the AWP with this precursor. Thus, it is necessary to search for other potential precursors serving to enhance the prediction skill of the AWP. Other than the tropical ENSO and local air–sea interactions, there are a limited number of studies that focus on the connection between extratropical signals and the AWP in the current literature, raising the question of whether the extratropical signals play a role.

Over the extratropical Pacific, the prolonged extreme SST warming events, also known as 'the Blob' [25], have received considerable research interests. Such extreme warming events can persist for years and impose huge impacts on the regional climate and ecosystem [26, 27]. During the recent decade, there are two prominent Blob events that occurred in 2013/2015 and 2019 [28, 29]. In the 2019 summer, remarkable SST warming took place in the northeastern Pacific with the SST anomalies close to 2.5 °C [28], raising considerable research interest in the summertime Blob. In recent advanced knowledge about the Blob, many studies have focused on its detection, driving mechanisms, and future prediction and projections [30, 31], but its local and remote impacts still require further investigations. It is suggested that the 2013/2015 Blob is connected with El Niño during the following winter in 2015/2016 via extratropical–tropical teleconnection [32]. Meanwhile, previous studies have suggested a tight connection between tropical Pacific and tropical Atlantic [13, 20, 33, 34]. Therefore, it attracts our research interest to investigate the variability of the Blob and its teleconnection with the tropical Atlantic basin. In the current literature, few studies investigated the relationship between the Blob and AWP, and the underlying mechanism is unclear. It is important to extend our understanding of the extratropical–tropical and Pacific–Atlantic teleconnections. In this study, a trans-basin teleconnection mechanism is introduced to explain the interannual variability of the AWP from an extratropical perspective. We intend to explore the lead–lag relationship between the summer Blob and the AWP, which may have implications for extending the predictability of the AWP to longer periods, other than the well-known ENSO.

2. Method

2.1. Data and index definitions

In this study, the atmospheric data (low sea surface pressure (SLP), geopotential height, and winds) are derived from NCEP/NCAR reanalysis 1 monthly mean dataset [35] for the period 1954–2018 on a 2.5 × 2.5 grid. The monthly SST data is derived from the NOAA Extended Reconstructed SST (ERSST) version 5 for the period 1954–2018 [36] with a spatial resolution of 2° × 2°. We also employ two other monthly SST datasets from the HadISST [37] and the COBE [38] to reexamine our results for the same period. The anomalies are calculated by removing the climatology for the period 1981–2010 from the monthly mean data. The net surface radiation data (defined to be positive downward) is derived from the NOC version 2.0 surface flux data set [39] for the period 1973–2014.

2.1.1. Blob index

The Blob index is defined as the area-weighted average of SST anomalies in a limited box over the northeastern Pacific (30°–60° N, 150°–120° W). The SST anomalies data is based on the ERSST version 5, as mentioned above. Previous studies also defined the Blob in a smaller area (40°–50° N, 150°–135° W) [28, 29]. The correlation of the two indices is 0.84 (significant at the 95% confidence level) for the period 1955–2017 (figure S1 (available online at stacks.iop.org/ERL/16/064034/mmedia)), indicating that the variability of the Blob index is not sensitive to the choice of area.

2.1.2. Atlantic warm pool index

The AWP index is defined by averaging SST anomalies in the region of Gulf of Mexico, the Caribbean Sea, and western tropical North Atlantic, which are usually regarded as the AWP region (10°–35° N, 100°–60° W) [40]. The SST data is also based on the ERSST. Our definition is consistent with the previous studies [13, 15].

2.1.3. Western hemisphere warm pool index

The WHWP index is derived from NOAA Physical Science Laboratory (https://psl.noaa.gov/data/correlation/whwp.data). The index is defined as the monthly anomaly of the ocean surface area warmer than 28.5 °C in the tropical Atlantic and eastern North Pacific [41]. This definition gives a better view of the warm pool changes in size, which reaches its maximum during the boreal summer and early fall while disappears in the winter [8, 42, 43]. The index is calculated based on HadISST and NOAA OI SST and the climatology is for the period 1971–2000. We introduce this index in a retrospective of the previous study [34, 41]. In this study, we find that the correlation between the WHWP and the AWP index reaches 0.86 and the lead–lag relationship of the Blob with the AWP index ($r = 0.68$) is as robust as with the WHWP index ($r = 0.64$) when the Blob leads by 1 year.

2.2. Model and experiment

The model we used in this study is the International Centre for Theoretical Physics AGCM version 41 (ICTPAGCM v41) [33] with a horizontal resolution of T30 (3.75° × 3.75°) with eight vertical levels. The ICTPAGCM is then coupled to a slab ocean thermodynamic mixed-layer model (SOM; no ocean dynamics are involved) with meridionally varying mixed-layer depth from 40 m (tropics) to 60 m (extratropics), considering the observed mixed-layer depth spatial variations.

In this study, we perform a model experiment to investigate the atmospheric responses to the Blob and the associated SST changes, referring to as the northeastern Pacific pacemaker experiment. The northeastern Pacific is prescribed with observed monthly varying SSTs derived from the ERSST, while outside the northeastern Pacific (30°–60° N, 180°–120° W), the ICTPAGCM is coupled to the SOM to reproduce the ocean–atmosphere interactions in response to the Blob forcing. In the SOM, the mixed-layer temperature is calculated based on net heat fluxes into the ocean, indicating that the simulated SSTs are forced by thermodynamic processes. Therefore, the simulated atmospheric circulation changes can be taken as combined effects directly generated from the Blob as well as the air–sea coupling outside the northeastern Pacific.

The northeastern Pacific pacemaker experiment is integrated for the period 1920–2018 and the first 34 years are for the model to spin up. We also restart the model with small initial perturbations to create five ensemble members. The ensemble means of simulated results from 1954 to 2018 are used for our analysis.

2.3. Statistical methods

2.3.1. Significance test

The two-tailed Student's t-test is used in this study to examine the statistical significance in the linear correlation analysis between two autocorrelated series. The effective number of degrees of freedom (N^{eff}) is given by:

$$\frac{1}{N^{\text{eff}}} \approx \frac{1}{N} + \frac{2}{N}\sum_{j=1}^{N}\frac{N-j}{N}\rho_{XX}(j)\,\rho_{YY}(j) \qquad (1)$$

where N denotes the sample size and $\rho_{XX}(j)$ stands for the autocorrelation of sampled time series X and $\rho_{YY}(j)$ is for Y, while j is the time lag.

2.3.2. The k-fold cross-validation

The k-fold cross-validation method [44] is used in this study to perform a hindcast for the AWP SST anomaly to examine the prediction capability of our Blob-based linear prediction model. We perform a ten-fold cross-validation method and divide the series into ten groups during the period 1956–2018. Each group is deleted and uses the remaining to construct the prediction model. Then, the deleted group is used to test the constructed prediction model.

3. Results

3.1. The Blob leads the AWP by 1 year

Figure 1(a) displays the regression map of the preceding year (JJA (−1)) SST anomalies onto the normalized summer (JJA (0)) AWP index (shading). There is a prominent warming signal over the Gulf of Alaska (green box in the Pacific) to the following year AWP. Its spatial pattern resembles the previous Blob studies [28, 29], indicating a potential linkage between them. Meanwhile, over the Intra-Americas Sea (green box in the Atlantic), the regression is rather weak, indicating the AWP warming has little relation with the preceding summer SST anomaly persistence. We also employ the correlation analysis (contour), which indicates a consistent strong warming signal in the northeastern Pacific. Therefore, we may conclude that the relationship between the AWP and the northeastern Pacific warming, referring to as the Blob, is robust and independent of the statistical analyses. Note that, for the remainder of this study, the time notions (0) refer that the season is in the same year as the AWP reaches its peak, while (−1) means the preceding year.

We also examine the time series of the Blob, WHWP, and AWP index for the periods 1955 (1956)–2017 (2018), with the Blob index led by 1 year (figure 1(b)). Both the Blob and WHWP indices

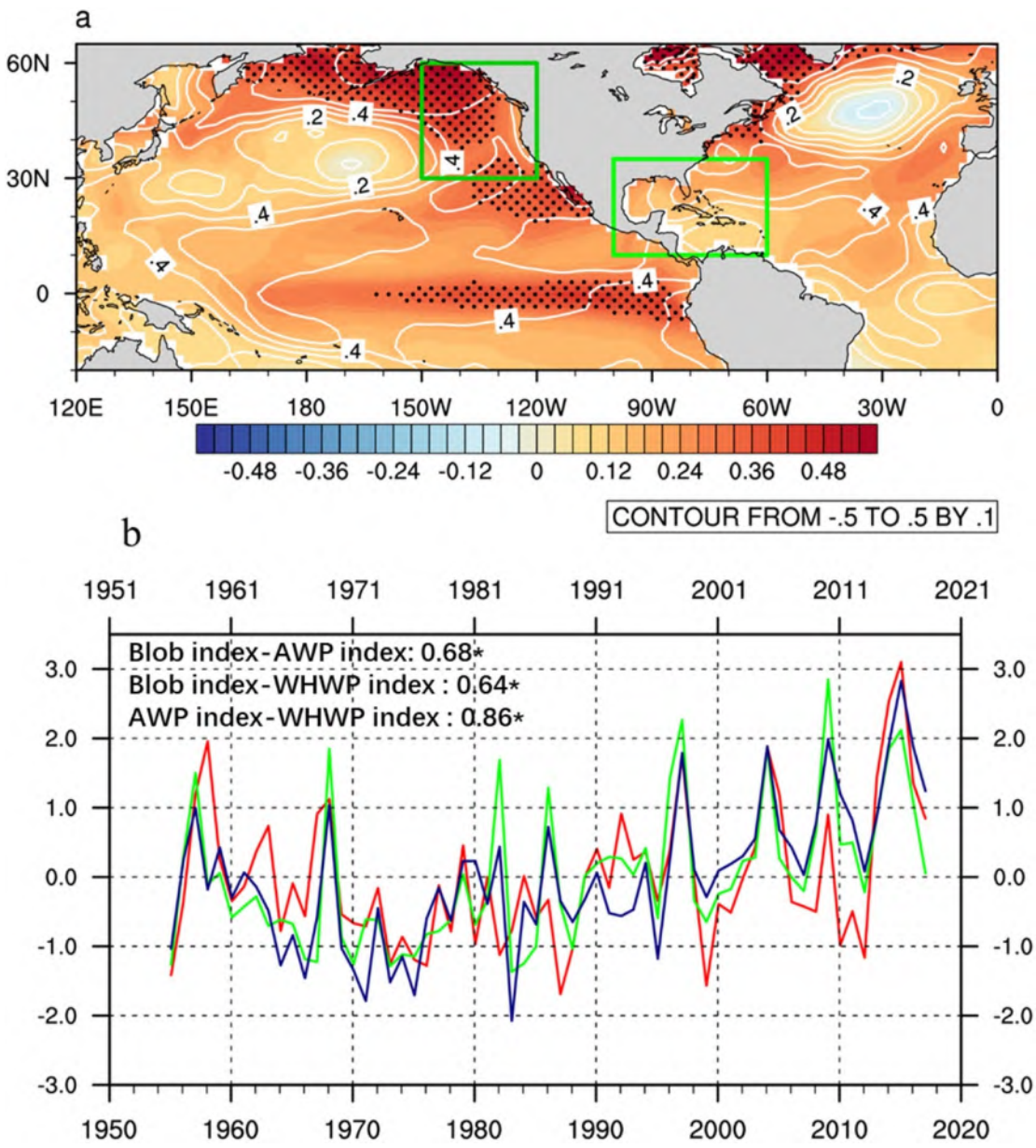

Figure 1. (a) Regression map (shading) of JJA (−1) SST anomalies (K) onto the normalized JJA (0) AWP index and correlation map (contour) between JJA (−1) SST anomalies (K) and the AWP index in JJA (0). The dotted shading indicates the regression is significant at the 95% confidence level. (b) Normalized time series of the Blob index (JJA (−1)) (red) for the period 1955–2017 (the bottom axis), WHWP index (green) and AWP index (JJA (0)) (blue) for the period 1956–2018 (the upper axis). The correlation coefficient with * means it is statistically significant at the 95% confidence level.

exhibit significant interannual variabilities, with 5–8 peaks during the analyzed period. In recent decades, the intensity and frequency of the Blob and WHWP witness consistent uprisings. The correlation coefficient reaches 0.64 ($r = 0.62$ and 0.65 in the HadISST and COBE SST, respectively), indicating a significant statistical connection between the Blob and the WHWP. In order to highlight the Atlantic counterpart, we further define the AWP index based on averaged SST anomaly in the limited area (10–35° N, 100–60° W; see the box in figure 2). The AWP index exhibits generally consistent variation with the WHWP index ($r = 0.86$) and also significantly correlates with the Blob ($r = 0.68$). We also use HadISST and COBE SST datasets to repeat our analysis and the correlation coefficient is still significant and reaches 0.63 and 0.65, respectively. This indicates that the relationship between the Blob and the warm pool is independent of index definitions and data selection. Moreover, the AWP index exhibits surprisingly well correspondence among the peak years with the preceding Blob in 1968–1969, 1997–1998, 2004–2005, and most recently 2015–2016. As shown in figure 1(b), the AWP index exhibits consistent slight warming trends and low-frequency (multi-decadal) variations. We further examine the relation-

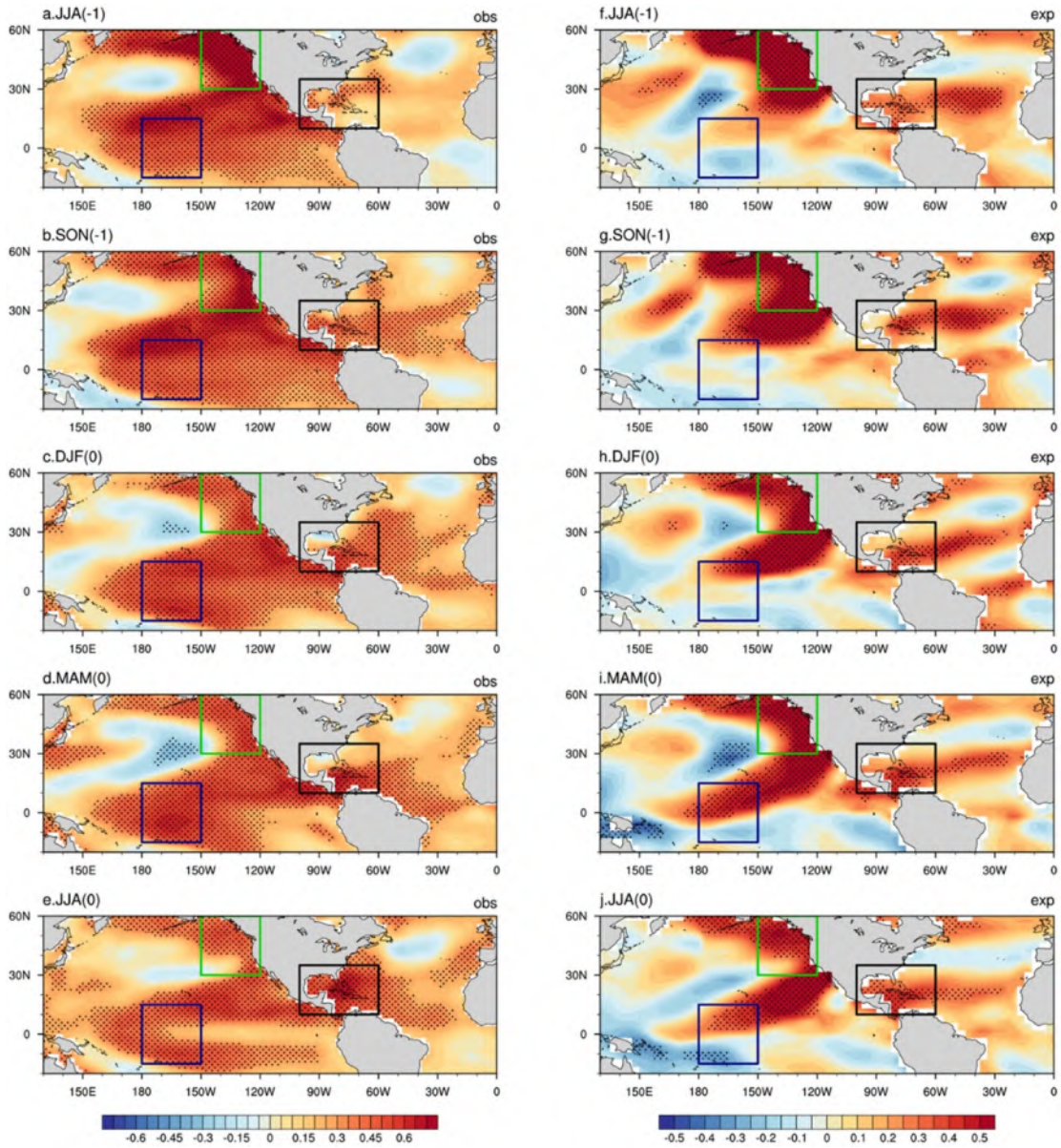

Figure 2. Correlations between the JJA (−1) Blob index and the SST anomalies from JJA (−1) to JJA (0) in both observation (a)–(e) and the northeastern Pacific pacemaker experiment (f)–(j). The green box is the area of Blob (30°–60° N, 150°–120° W). The black box is the area of AWP (10°–35° N, 100°–60° W). The blue box is the area of central Pacific (15° S–15° N, 180°–150° W). The dotted area represents the correlation is statistically significant at the 95% confidence level.

ship between the Blob and AWP using detrended data (figure S2 (available online at stacks.iop.org/ERL/16/064034/mmedia)). The 1 year lead relationship between the Blob and the AWP barely changes, as the correlation coefficient reaches 0.66. We also calculate the correlation with their low-frequency variations removed (with the 21 year running mean subtracted from them) (figure S3 online), and the connection remains. ($r = 0.62$, significant at the 95% confidence level). It indicates the Blob–AWP relationship is independent of the low-frequency variation or the linear warming trend. The above spatial and temporal analysis reveals an unseen linkage between the North Pacific Blob and the AWP at a time lag of 1 year, but the evolution of the Blob signal into the AWP region requires further inspections.

Figure 2(a) depicts the spatial distribution of the Blob in JJA (−1) by correlating its index with the simultaneous SSTs. The most prominent warming occurs in the northeastern Pacific and extends southwestward, which is similar to the pattern in the previous case study of the Blob in the summer of 2019 [28]. However, the AWP response is rather weak and shows no significant correlation with the Blob, suggesting the relationship between them is unlikely to be simultaneous. The intensity of the Blob abruptly weakens after peaking in JJA (−1) and the anomalous warm water contracts toward the coast and the tropics during the preceding fall (SON (−1)) (figure 2(b)). While the Blob is continuously weakening, the anomalous warming center has moved southwestward to the central Pacific throughout the winter

(DJF (0)) (figure 2(c)) and reaches its maximum in the next spring (MAM (0)) (figure 2(d)). For the AWP region, it starts to warm up since SON (−1), but the correlation between the JJA (−1) Blob and SON (−1) AWP is only close to 0.5. In the following seasons, the correlations become stronger since DJF (0), indicating that there is a significant warming tendency of AWP in response to the preceding JJA (−1) Blob. The SST warming continuously enhances and eventually reaches the peak in JJA (0). During the peak season, the AWP exhibits the most prominent warming response to the preceding Blob. The range of the AWP also reaches its maximum, covering the areas of the Caribbean Sea, Gulf of Mexico, and further extending to the tropical North Atlantic as well as midlatitudes. By contrast, the warming center over the central Pacific significantly weakens during JJA (0), together with rather weak responses over the equatorial eastern Pacific (not significant). We also reexamine the correlation pattern in JJA (0) based on the HadISST and COBE SST data (figure S4 online). The correlation maps are overall consistent with that using the ERSST dataset, exhibiting strong AWP warming in response to the preceding Blob. Therefore, the lead–lag relation between them is robust and independent with data selection.

Based on the above analyses, we determine three key regions located over the North Pacific (where the Blob is defined), Intra-Americas Sea (where the AWP is defined), and central Pacific. Considering the fact that the DJF (0) central Pacific SST exhibits strong warming responses to the preceding Blob and leads AWP SST warming in the following year, the central Pacific may play an intermedia role in the Blob–AWP teleconnection. Therefore, we select the area that is used to define the central Pacific SST anomaly based on the DJF (0) SST correlation maps with both the JJA (−1) Blob and JJA (0) AWP indices. In light of the results (figures are not shown here), we find that over 15° S–15° N and 180°–150° W, the correlations of tropical SST with the following season AWP index and the preceding season Blob index are consistently prominent.

We then calculated the lead–lag correlations of the JJA (−1) Blob index with the central Pacific index (SST averaged over 15° S–15° N and 180°–150° W) and the AWP index over different seasons. As shown in figure 3(a), the central Pacific region is witnessed by continuous warming after SON (−1) and reaches the peak during MAM (0) ($r = 0.64$). Corresponding to the spatial evolution in figures 2(c)–(d), the anomalous warming signal in response to the preceding summer Blob has now moved into the central Pacific region. As for the AWP region, the preceding Blob does not correlate with the contemporary AWP SST very well ($r = 0.34$), but the response intensifies during MAM (0), following the prior warming in the central Pacific at a time lag of one or two seasons. Interestingly, the central Pacific and AWP SSTs, without direct oceanic 'tunnel', share a consistent warming trend, implying a potential 'bridge' in the atmosphere. In JJA (0), the AWP SST warming in response to the former Blob reaches the maximum ($r = 0.68$), indicating a second shift of the warming center. The above spatial and temporal analysis reveals a statistically significant connection between the former Blob and the AWP with a time lag of approximately 1 year.

Based on the above analyzes, we can infer that the central Pacific SST may play an intermediate role in this trans-basin teleconnection. On the other hand, previous studies have pointed out that the tropical central Pacific SST variation is able to exert extreme northeastern Pacific SST anomalies [28, 29]. In addition, the seasonal persistence of central Pacific SST anomalies may also impose an influence on the Blob–AWP teleconnection. It brings the question: whether the Blob–AWP teleconnection is only induced by the Blob? To address this issue, we calculate the correlation between the detrended JJA (−1) central Pacific SST index and the JJA (0) AWP index. The correlation coefficient only reaches 0.40, which is much smaller than the lead correlation between the detrended JJA (−1) Blob and JJA (0) AWP ($r = 0.66$). The AWP variance explained by the JJA (−1) Blob is twice larger than that by the JJA (−1) central Pacific SST. Also, the two time series barely match (figure S5 online), indicating the summertime central Pacific SST variation has limited influence on the following AWP. The partial correlation between JJA (−1) central Pacific SST and JJA (0) AWP with the JJA (−1) Blob index removed is reduced to 0.07, highlighting a critical role of the Blob. Moreover, the correlation between the JJA (−1) Blob and JJA (0) AWP is still significant after removing the JJA (−1) central Pacific SST index (partial correlation $r = 0.58$). Therefore, we may conclude that the Blob–AWP teleconnection is not dominated by the JJA (−1) central Pacific SST variation and independent of its seasonal persistence. Instead, the DJF (0) central Pacific SST exhibits strong warming responses to the preceding Blob ($r = 0.59$) and significant lead correlation with the following AWP ($r = 0.54$), further confirming an intermedia role of the central Pacific SST in transmitting the preceding Blob signal into the AWP region.

The above observational analysis only suggests a statistically robust relationship, but their connection from the physical perspective requires further inspection. We then carry out the Northeast Pacific pacemaker experiment to investigate the SST evolution forced by the simulated atmospheric response to the preceding Blob. In JJA (−1), the correlation map (figure 2(f)) is similar to that observed over the Northeast Pacific and 'arc-shaped' warming corresponds well with the Blob. In the following seasons (figures 2(g)–(j)), the simulated evolution of Pacific

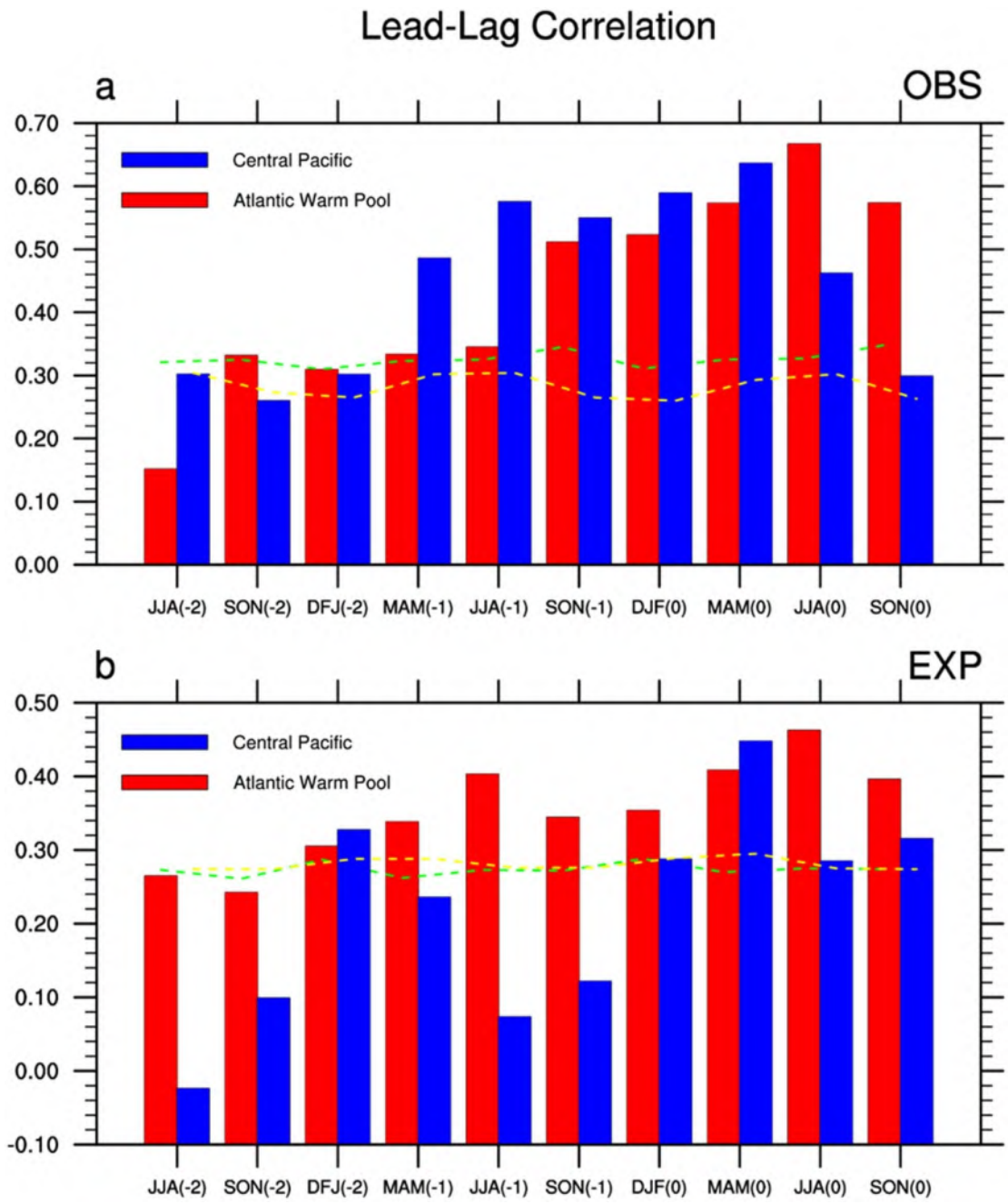

Figure 3. The lead–lag correlations between JJA (−1) Blob index (1955–2017) and AWP index (red) and central Pacific index (blue) (1956–2018), respectively. (a) is for the observation and (b) is for the northeastern Pacific pacemaker experiment. The threshold corresponding to the 95% confidence level for the correlations is marked in the figure (the yellow dash line is for the central Pacific; the green dash line is for the AWP).

SST anomalies associated with the Blob is overall consistent with the observation. The most prominent feature is that a 'warm tongue' stretches southwestward from the northeastern Pacific to the central Pacific, accompanied by the decaying Blob. Consistent with the observation, the central Pacific region experiences a continuous warming process towards the tropics, together with the warm ridge extending far west.

As shown in figure 3(b), the correlation coefficients between the Blob and central Pacific SST, after touching the bottom in JJA (−1), constantly rise till peaking ($r = 0.45$) in MAM (0), indicating that the model well reproduces the first shift of the warming center inside the Pacific Ocean basin. The pacemaker experiment aims to understand how the SST reacts to the Blob-related anomalous atmospheric forcing. Thus the extension of the Northeast Pacific 'warm tongue' is likely forced by the thermodynamic process. However, the model seems unable to reproduce the warming response in the western North Pacific and the Southern Hemisphere tropics, indicating these anomalous signals may be model biases or they may not be directly related to the Blob-induced thermodynamic forcing.

In the Atlantic Ocean, the simulated response of AWP SST to the Blob is moderate in JJA (−1) and persists till the next season (figures 2(f) and (g)), but significant warming can be found over the subtropical region while a 'warm hole' is locating at midlatitudes, consistent with the observation (figure 2(a)). Entering DJF (0), warm water over the Caribbean Sea develops (figure 2(h)), but in general, the AWP response is still weak during this period (figure 3(b)). Abrupt warming in the AWP region takes place in MAM (0) and constantly strengthens afterward. In JJA (0), the AWP reaches its maximum intensity in response to the preceding Blob ($r = 0.46$), with the largest extent of warm water covering the Intra-Americas Sea. Based on the above analyses, both observation and model simulation indicate a robust relationship between the AWP and the preceding Blob. The pacemaker experiment generally captures the southwestward SST evolution in the North Pacific Ocean from JJA (−1) to MAM (0) and the warm water development in the AWP region from DJF (0) to JJA (0). More importantly, the time lag of warming peaks between the central Pacific and AWP SST is well simulated. It indicates that the Blob-related thermodynamic processes are responsible for the SST evolution in each ocean and the trans-basin coherence.

3.2. Role of seasonal footprint mechanism

We inspect the anomalous atmospheric circulation in response to the preceding summer Blob by regressing the SLP and wind anomalies onto the normalized Blob index. In the reanalysis, the strong Blob (SST footprint) corresponds with an anomalous low SLP and the associated cyclonic circulation over the North Pacific midlatitudes (figure 4(a)). In response to the SLP decline, anomalous westerly winds are found in the subtropical central Pacific region, south to the low-pressure. Such anomalous westerlies related to the Blob weaken the trade winds, preventing heat loss from the surface due to the depressed evaporation and driving the Northeast Pacific SST footprint towards the equator. For the following seasons, the westerlies accompanied by the low SLP continuously move southward, resulting in the SST warming towards the tropical central Pacific region. This process largely resembles the seasonal footprint mechanism (SFM) proposed by the previous studies [45, 46]. In DJF (0) (figure 4(c)), the subtropical low-pressure center strongly intensifies due to the underlying SST warming. During the spring (figure 4(d)), the tropical central Pacific is governed by anomalous high pressure corresponded with the subtropical pressure decline, indicating a weakened Hadley circulation. Such a weakened meridional circulation induces anomalous westerlies along both sides of the equator, amplifying the central Pacific SST warming and generating a symmetric pattern in the tropics.

In the North Pacific pacemaker experiment, those observed features are reproduced to a large extent. In JJA (−1), the low-pressure corresponds with the northeastern Pacific SST warming and induces strong southwesterly winds converging to the Blob (figure 4(f)). The westerlies constantly exhibit equatorward movement, consistent with the simulated 'warm tongue' extension (figure 4(g)). During the DJF (0) (figure 4(h)) and MAM (0) (figure 4(i)), a weakened Hadley circulation can be found and the anomalous symmetrical divergence flows along the equator strongly intensify the warming over the tropical central Pacific, consistent with the reanalysis. The above analyses indicate an important role of Blob-related thermodynamic processes in the evolution of the North Pacific 'warm tongue'. It explains that the tropical central Pacific warming is largely due to the extratropical Blob signal through the SFM, consistent with previous studies [47, 48].

3.3. Role of local air–sea feedback

However, without direct oceanic ventilation to the Blob, the driving mechanism of the AWP warming is more likely associated with the local air–sea feedback. In the preceding year (JJA (−1)), the AWP region exhibits high SLP anomalies accompanied by the weak divergent circulation in response to the Blob and the contemporary AWP SST warming is relatively weak (figure 4(a)). As shown in figure 4(b), an anomalous low-pressure associated with the preceding Blob emerges in the warm pool region in SON (−1) when the AWP starts to warm up. Then, the low-pressure anomaly develops substantially in the Gulf region since DJF (0) (figure 4(c)) and further persists throughout MAM (0) and JJA (0), leading the rapid SST warming over the AWP region. Therefore, the low-pressure anomaly in the AWP region is likely a key factor that boots the SST warming through local air–sea interactions.

The cyclonic circulation induces anomalous ascending motions over the AWP region, which further increases the local cloudiness and prevents heat loss by increasing the downward longwave radiation (LWR), referring to as SST–SLP–cloud–LWR positive feedback. We further examine the correlations of JJA (−1) Blob with the net surface LWR and short-wave radiation (SWR) over four successive seasons (MAM (0)–JJA (0)) (figure S6 online). The LWR and SWR generally exhibit opposite responses to the preceding Blob signal over the AWP region. This is consistent with the Blob-associated low-pressure anomalies in MAM (0), which increase the cloudiness over the AWP region. As shown in figure S6, the LWR persistently contributes to the AWP SST warming, while in contrast, the SWR is negatively correlated with preceding Blob during four successive seasons, suggesting that the SWR has a damping effect on the development of underlying SST warming, rather than a

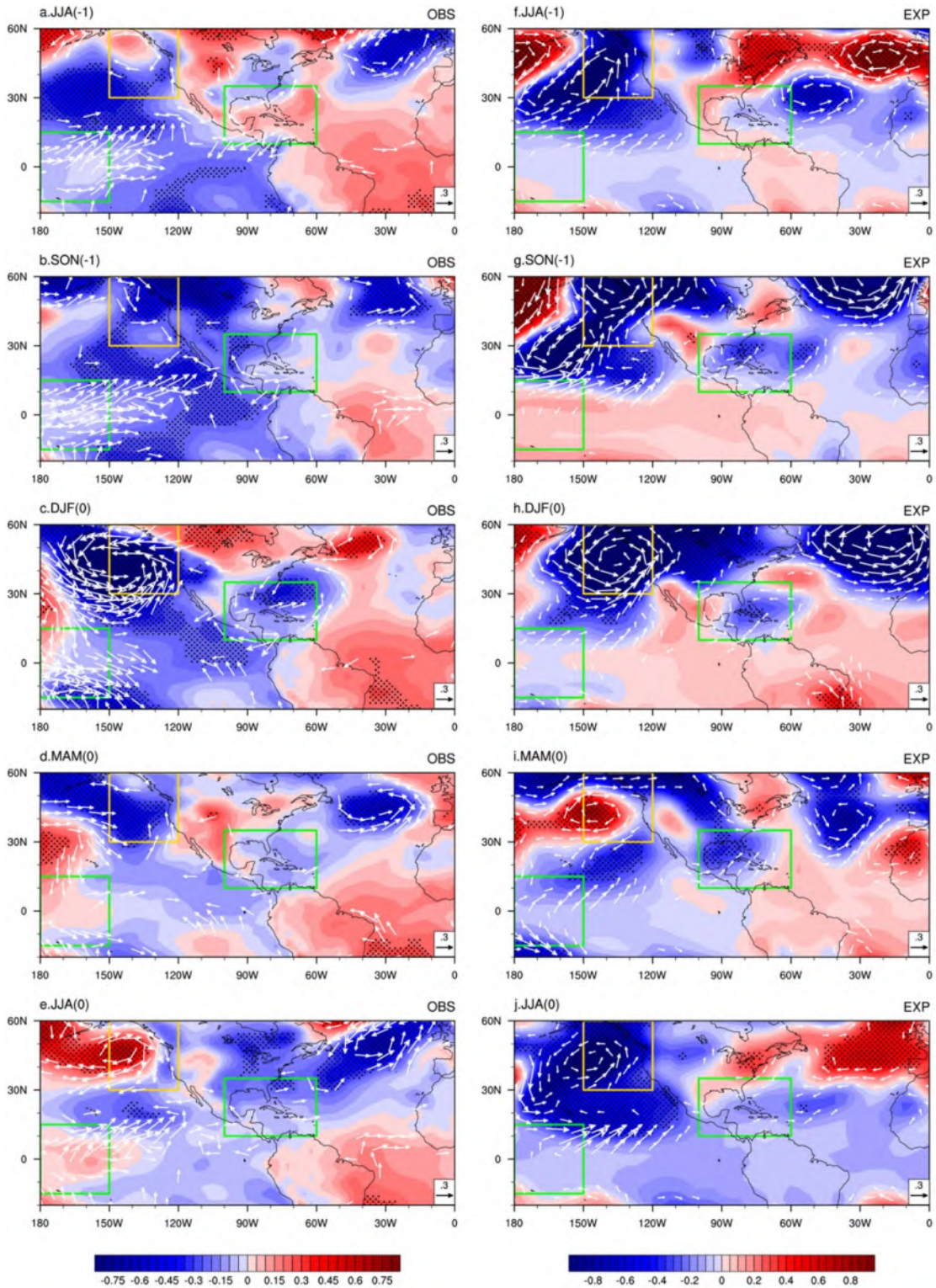

Figure 4. Regressions of the SLP (hPa) and wind anomalies (m s^{-1}) onto the normalized JJA (−1) Blob index from JJA (−1) to JJA (0) in both observation (a)–(e) and the northeastern Pacific pacemaker experiment (f)–(j). The dotted shading indicates the regression is significant at the 95% confidence level. Only vector trends significant at the 90% confidence level are shown in the figures.

forcing effect. The area-averaged LWR exhibits relatively high correlations with the Blob over all selected seasons, stronger and more significant than the SWR (figure S7 online). Based on the above analysis, we may conclude that the LWR plays a more important role in forcing the AWP SST warming and linking the AWP warming with the preceding Blob. The increase in the net surface downward LWR is consistent with the AWP SST warming and further results in the persistent development of the warm SST anomaly of AWP in summer (figure 2). Our results are consistent with the previous study [34], which suggested that

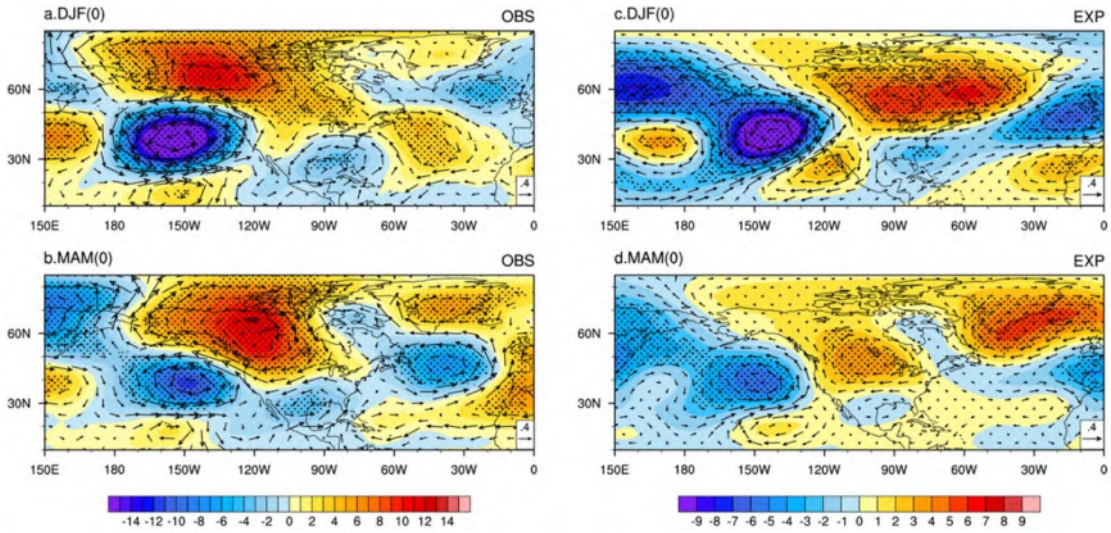

Figure 5. Regressions of 500 hPa geopotential height (m) and wind anomalies (m s^{-1}) onto the normalized JJA (−1) Blob index. (a) and (b) are for observation in DJF (0) and MAM (0), respectively, while (c) and (d) are for the northeastern Pacific pacemaker experiment. The dotted shading indicates the regression is significant at the 95% confidence level.

the SST–SLP–cloud–LWR positive feedback plays a dominant role in the development of AWP SST anomaly. In addition, the westerly winds along with the low-pressure weaken the northeast trade winds over the AWP, reduce surface evaporation and prevent latent heat loss, resulting in strong SST warming (wind–evaporation–SST feedback) [19].

We also inspect the evolution of SLP over the AWP region in the model simulation. Consistent with the reanalysis, anomalous low SLP is found over the AWP from DJF (0) to JJA (0) accompanied by the relatively strong westerlies that stimulate the wind–evaporation–SST feedback to heat the underlying ocean (figures 4(h)–(j)). The critical low SLP reaches its maximum intensity during the spring. The strong ascending motions favor the increase in cloudiness and the associated SST–SLP–cloud–LWR positive feedback, further amplifying the AWP warming. The simulated net surface LWR/SWR patterns (figure S8 online) also suggest that the LWR dominates the SST warming, consistent with the observation. This indicates that the SST–SLP–cloud–LWR positive feedback is well reproduced in the model, confirming the key role of local air–sea feedback in the development of AWP SST anomaly. Note that although the low-pressure anomaly is weakened during JJA (0), the summertime convection and lagged SST response to the preceding thermodynamic feedbacks can also explain the simulated SST peak in the AWP region, which agrees with the reanalysis. From the above, we have addressed how the Blob-related 'warm tongue' evolves to the central Pacific and how the AWP SST warming interacts with the low SLP anomalies. In both ocean basins, the thermodynamic feedbacks are keys to the SST evolution, as shown in both reanalysis and model simulation. However, the connection between the formation of the low SLP anomalies in the AWP and the preceding Blob warming remains unexplored.

3.4. Inter-basin atmospheric teleconnection

We further calculate the correlation coefficient between the central Pacific SST (MAM (0)) and the AWP SST (JJA (0)) that reaches 0.56, indicating a close trans-basin connection exists, with the central Pacific SST leading by approximately one season. However, the partial correlation decreases to 0.23 without considering the effect of the preceding Blob. We may infer that the relationship between them is associated with the Blob. Further, it is likely that the preceding Blob induces SST variations over both the central Pacific and the AWP during the following seasons. Based on the above analyses, the atmospheric teleconnection may play a role between the central Pacific and the AWP. Figure 5 displays the 500 hPa geopotential height anomalies regressed onto the normalized Blob index during the DJF (0) and MAM (0) in the reanalysis and pacemaker experiment. The regression map exhibits the Pacific/North American (PNA) teleconnection pattern [49, 50] in response to the preceding summer Blob. A trans-basin teleconnection mechanism is proposed here. The preceding summer Blob signal evolves equatorward through the SFM, inducing the SST warming over the equatorial central Pacific, which further excites the PNA teleconnection pattern to a large extent. The Blob itself also shows persistence from DJF (0) to MAM (0) and may therefore directly contribute to the PNA teleconnection. The PNA pattern consists of three alternatively distributed geopotential height anomalies centers located over the northeastern Pacific (negative), North America (positive), and Gulf of Mexico (negative). Following the great circle path, the anomalous central Pacific SST warming signal can

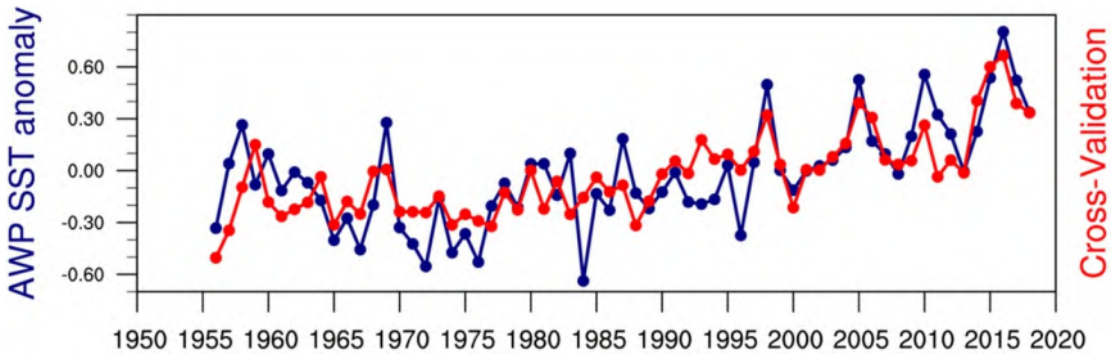

Figure 6. Time series of the AWP SST anomalies in the observation (blue line) and hindcast (red line), respectively. The hindcast SST anomaly is calculated using the *k*-fold cross-validation method based on the Blob-based linear prediction model (see main text for details).

be transported across the North American continent and induces anomalous low SLP in the AWP, which has been proved to be an essential background that is favorable to the AWP SST warming. The existence of the low-pressure anomaly over the AWP region corresponds well with the development of the PNA patter during the winter. In MAM (0) (figure 5(b)), the PNA pattern is weakened but still exists with a bit eastward shift. It is important to maintain the low-pressure anomalies in the AWP region and enhance the associated feedback for the SST warming till JJA (0). The Northeast Pacific pacemaker experiment also exhibits the consistent PNA pattern in the winter (figure 5(c)) and spring (figure 5(d)), indicating the inter-basin teleconnection in response to the preceding Blob is reasonably reproduced in the model. Therefore, we may conclude that the PNA pattern explains how the low-pressure is formed and plays an important role in connecting the central Pacific and the AWP SST, consistent with the previous study [51].

3.5. The Blob-based prediction model for the AWP

Based on the above analysis, the Blob shows great implications for predicting the AWP 1 year in advance. A linear regression model is constructed based on the preceding Blob index and is shown as follows:

$$\mathrm{AWP}\,(t) = a_1 \mathrm{Blob}\,(t-1) + a_2 t + a_0 \qquad (2)$$

where a_1, a_2 and a_0 are the coefficients, while Blob and t denote the Blob index and time in years, respectively. As shown in figure 1(b), the AWP exhibits a slight warming trend, indicating a contribution from global warming denoted as $a_2 t$ in the model. Furthermore, the *k*-fold cross-validation method (see section 2) is used here to examine the prediction capability of the linear model and has also been employed in the previous study [52]. The hindcast of the AWP SST anomalies for the period 1956–2018 is shown in figure 6 and the correlation coefficient between the hindcast and the observed AWP series reaches 0.76 (significant at the 95% confidence level). The hindcast results are insensitive to the low-frequency variations in the time series (figure S3). After removing the low-frequency component, the correlation coefficient between the observed AWP and hindcast remains significant ($r = 0.57$, significant at the 95% confidence level). The cross-validated AWP SST anomaly is generally consistent with that observed, further indicating that the Blob is a useful predictor for the AWP 1 year in advance.

4. Discussion and conclusion

During the recent decades, the AWP has received considerable attention since its impacts on the American and western European weather and climate are non-negligible. In this study, we find an unrevealed factor that leads the AWP by 1 year from the extratropical North Pacific, called the Blob (lead–lag $r = 0.68$). It has been identified as a prolonged extreme ocean warming event that has great impacts on regional climate and ecosystems, but its relation with the AWP has not been fully documented in the literature. Our analyses suggest that the preceding summer (JJA (−1)) Blob induces strong westerly wind anomalies, which further transmit the anomalous warming signal towards the central Pacific through the SFM. The central Pacific SST warming has substantially developed since DJF (0) and reaches its peak intensity in MAM (0). Meanwhile, the PNA teleconnection is established, accompanied by tropical Pacific warming. At the downstream of the wave train, the AWP region exhibits significant low SLP anomalies, which plays an important role in the SST warming. South to the low-pressure, strong westerlies compensate the northeast trade winds, triggering the wind–evaporation–SST feedback to heat the underlying ocean. Moreover, the corresponding convergence and ascending motions increase the local cloudiness, preventing heat loss by enhancing the downward net surface LWR, which dominates the

AWP warming. Entering the summer, the initial SST warming together with favorable conditions for deep convection reinforces the SST–SLP–cloud–LWR positive feedback and consequently leads to the warming peak over the AWP in response to the preceding Blob. The Northeast Pacific pacemaker experiment reasonably well reproduces the above mechanism and the atmospheric responses are somewhat agreed with the reanalysis, indicating that the thermodynamic process plays a dominant role in the teleconnection between the AWP and the preceding Blob.

Our findings considerably extend the AWP predictability to a longer period of time, comparing to the previous ENSO as a precursor. We further examine the partial correlation between the preceding summer Blob and the AWP with the preceding winter ENSO signal (Niño 3.4) removed (partial correlation $r = 0.58$). This indicates that the Blob–AWP connection we found in this study is not dominated by the ENSO. In addition, an ENSO-based AWP prediction model (see supplementary material) is constructed for better comparison (figure S9 online). The ENSO-based hindcast show less skill in capturing the key interannual features of the observed AWP variability, probably due to the weaker coherence between ENSO and AWP at interannual timescales ($r = 0.45$). In the current study, we use the thermodynamic slab ocean model to investigate the mechanism between the Pacific Blob and the AWP. Previous studies have suggested the ocean dynamics also play a role in the Pacific–Atlantic connections [21, 23]. Therefore, future works are required to employ a dynamic ocean model in the pacemaker experiment.

Moreover, a recent study has pointed out that the high impact extreme SST warming event (e.g. the Blob) is attributed to anthropogenic global warming [53]. Additionally, more frequent and intense SST warming events are projected in the future [54]. Therefore, it is worth knowing how the Blob–AWP teleconnection pattern is changed under the circumstances of global warming and whether a stronger Blob corresponds to a proportionally intensified AWP.

Data availability statement

All data that support the findings of this study are included within the article (and any supplementary files).

Acknowledgments

This work was jointly supported by the National Natural Science Foundation of China (41975082, 41775038, 41731173 and 41790474), National Key Research and Development Program of China (2016YFA0601801 and 2019YFA0606701) and the National Programme on Global Change and Air–Sea Interaction (GASI-IPOVAI-06 and GASI-IPOVAI-03).

ORCID iDs

Cheng Sun https://orcid.org/0000-0003-0474-7593
Jianping Li https://orcid.org/0000-0003-0625-1575

References

[1] Drumond A, Nieto R and Gimeno L 2011 On the contribution of the tropical western hemisphere warm pool source of moisture to the northern hemisphere precipitation through a Lagrangian approach *J. Geophys. Res.: Atmos.* **116** 1–9
[2] Gimeno L, Drumond A, Nieto R, Trigo R M and Stohl A 2010 On the origin of continental precipitation *Geophys. Res. Lett.* **37** L13804
[3] Gimeno L, Nieto R, Drumond A, Durán-Quesada A M, Stohl A, Sodemann H and Trigo R M 2011 A close look at oceanic sources of continental precipitation *EOS, Trans. Am. Geophys. Union* **92** 193–4
[4] Gimeno L, Nieto R, Trigo R M, Vicente-Serrano S M and López-Moreno J I 2010 Where does the Iberian peninsula moisture come from? An answer based on a Lagrangian approach *J. Hydrometeorol.* **11** 421–36
[5] Sorí R, Drumond A and Nieto R 2015 Moisture contribution of the Atlantic warm pool to precipitation: a Lagrangian analysis *Front. Environ. Sci.* **3** 22
[6] Misra V, Moeller L, Stefanova L, Chan S, O'Brien J J, Smith T J and Plant N 2011 The influence of the Atlantic warm pool on the Florida panhandle sea breeze *J. Geophys. Res.: Atmos.* **116** D00Q06
[7] Taylor M A, Enfield D B and Chen A A 2002 Influence of the tropical Atlantic versus the tropical Pacific on Caribbean rainfall *J. Geophys. Res.: Oceans* **107** 1011–4
[8] Wang C, Enfield D B, Lee S-K and Landsea C W 2006 Influences of the Atlantic warm pool on western hemisphere summer rainfall and Atlantic hurricanes *J. Clim.* **19** 3011–28
[9] Wang C and Lee S 2007 Atlantic warm pool, Caribbean low-level jet, and their potential impact on Atlantic hurricanes *Geophys. Res. Lett.* **34** L02703
[10] Enfield D B and Cid-Serrano L 2010 Secular and multidecadal warmings in the north Atlantic and their relationships with major hurricane activity *Int. J. Climatol.* **30** 174–84
[11] Wang C and Lee S-K 2007 Impact of the Atlantic warm pool on the summer climate of the western hemisphere *J. Clim.* **20** 5021–40
[12] Wang C, Lee S-K and Enfield D B 2008 Atlantic warm pool acting as a link between Atlantic multidecadal oscillation and Atlantic tropical cyclone activity *Geochem. Geophys. Geosyst.* **9** Q05V03
[13] Park J-H *et al* 2018 Predicting el niño beyond 1 year lead: effect of the western hemisphere warm pool *Sci. Rep.* **8** 1–8
[14] Park J-H, Kug J-S, An S-I and Li T 2019 Role of the western hemisphere warm pool in climate variability over the western north Pacific *Clim. Dyn.* **53** 2743–55
[15] Park J-H, Li T, Yeh S-W and Kim H 2019 Effect of recent Atlantic warming in strengthening Atlantic–Pacific

teleconnection on interannual timescale via enhanced connection with the Pacific meridional mode *Clim. Dyn.* **53** 371–87
[16] Wang C, Lee S-K and Mechoso C R 2010 Interhemispheric influence of the Atlantic warm pool on the southeastern Pacific *J. Clim.* **23** 404–18
[17] Lee S-K, Enfield D and Wang C 2007 What drives the seasonal onset and decay of the western hemisphere warm pool? *J. Clim.* **20** 2133–46
[18] Chang P, Ji L and Li H 1997 A decadal climate variation in the tropical Atlantic ocean from thermodynamic air–sea interactions *Nature* **385** 516–8
[19] Xie S P and Philander S G H 1994 A coupled ocean-atmosphere model of relevance to the ITCZ in the eastern Pacific *Tellus* A **46** 340–50
[20] Cai W *et al* 2019 Pantropical climate interactions *Science* **363** eaav4236
[21] Enfield D B and Mayer D A 1997 Tropical Atlantic sea surface temperature variability and its relation to el niño-southern oscillation *J. Geophys. Res.: Oceans* **102** 929–45
[22] Hastenrath S 2000 Upper air mechanisms of the southern oscillation in the tropical Atlantic sector *J. Geophys. Res.: Atmos.* **105** 14997–5009
[23] Klein S A, Soden B J and Lau N-C 1999 Remote sea surface temperature variations during enso: evidence for a tropical atmospheric bridge *J. Clim.* **12** 917–32
[24] Enfield D B, Lee S-K and Wang C 2006 How are large western hemisphere warm pools formed? *Prog. Oceanogr.* **70** 346–65
[25] Bond N A, Cronin M F, Freeland H and Mantua N 2015 Causes and impacts of the 2014 warm anomaly in the NE Pacific *Geophys. Res. Lett.* **42** 3414–20
[26] Holbrook N J *et al* 2019 A global assessment of marine heatwaves and their drivers *Nat. Commun.* **10** 1–13
[27] Wernberg T, Smale D A, Tuya F, Thomsen M S, Langlois T J, De Bettignies T, Bennett S and Rousseaux C S 2013 An extreme climatic event alters marine ecosystem structure in a global biodiversity hotspot *Nat Clim. Change* **3** 78–82
[28] Amaya D J, Miller A J, Xie S-P and Kosaka Y 2020 Physical drivers of the summer 2019 north Pacific marine heatwave *Nat. Commun.* **11** 1–9
[29] Di Lorenzo E and Mantua N 2016 Multi-year persistence of the 2014/15 north Pacific marine heatwave *Nat Clim. Change* **6** 1042–7
[30] Benthuysen J A, Oliver E C J, Chen K and Wernberg T 2020 Editorial: advances in understanding marine heatwaves and their impacts *Front. Mar. Sci.* **7** 147
[31] Oliver E C J *et al* 2019 Projected marine heatwaves in the 21st century and the potential for ecological impact *Front. Mar. Sci.* **6** 734
[32] Tseng Y-H, Ding R and Huang X-M 2017 The warm Blob in the northeast Pacific—the bridge leading to the 2015/16 El Niño *Environ. Res. Lett.* **12** 054019
[33] Kucharski F, Parvin A, Rodriguez-Fonseca B, Farneti R, Martin-Rey M, Polo I, Mohino E, Losada T and Mechoso C R 2016 The teleconnection of the tropical Atlantic to indo-Pacific sea surface temperatures on inter-annual to centennial time scales: a review of recent findings *Atmosphere* **7** 29
[34] Wang C and Enfield D B 2003 A further study of the tropical western hemisphere warm pool *J. Clim.* **16** 1476–93
[35] Kalnay E *et al* 1996 The ncep/ncar 40 year reanalysis project *Bull. Am. Meteorol. Soc.* **77** 437–71
[36] Huang B, Thorne P W, Banzon V F, Boyer T, Chepurin G, Lawrimore J H, Menne M J, Smith T M, Vose R S and Zhang H-M 2017 Extended reconstructed sea surface temperature, version 5 (ERSSTv5): upgrades, validations, and intercomparisons *J. Clim.* **30** 8179–205
[37] Rayner N *et al* 2003 Global analyses of sea surface temperature, sea ice, and night marine air temperature since the late nineteenth century *J. Geophys. Res.: Atmos.* **108** 4407
[38] Ishii M *et al* 2016 Objective analyses of sea-surface temperature and marine meteorological variables for the 20th century using ICOADS and the Kobe Collection *Int. J. Climatol.* **7** 865–79
[39] Berry D I and Kent E C 2011 Air-sea fluxes from icoads: the construction of a new gridded dataset with uncertainty estimates *Int. J. Climatol.* **31** 987–1001
[40] Wang C, Liu H, Lee S-K and Atlas R 2011 Impact of the Atlantic warm pool on united states landfalling hurricanes *Geophys. Res. Lett.* **38** L19702
[41] Wang C and Enfield D B 2001 The tropical western hemisphere warm pool *Geophys. Res. Lett.* **28** 1635–8
[42] Gimeno L, Magaña V and Enfield D B 2011 Introduction to special section on the role of the Atlantic warm pool in the climate of the western hemisphere *J. Geophys. Res.: Atmos.* **116** D00Q01
[43] Liu H, Wang C, Lee S-K and Enfield D 2015 Inhomogeneous influence of the Atlantic warm pool on United States precipitation *Atmos. Sci. Lett.* **16** 63–9
[44] Michaelsen J 1987 Cross-validation in statistical climate forecast models *J. Appl. Meteorol. Climatol.* **26** 1589–600
[45] Vimont D J, Battisti D S and Hirst A C 2001 Footprinting: a seasonal connection between the tropics and mid-latitudes *Geophys. Res. Lett.* **28** 3923–6
[46] Vimont D J, Wallace J M and Battisti D S 2003 The seasonal footprinting mechanism in the Pacific: implications for ENSO *J. Clim.* **16** 2668–75
[47] Chen S, Wu R, Chen W and Yu B 2015 Influence of the november arctic oscillation on the subsequent tropical Pacific sea surface temperature *Int. J. Climatol.* **35** 4307–17
[48] Ding R *et al* 2019 Relative contributions of north and south Pacific sea surface temperature anomalies to ENSO *J. Geophys. Res.: Atmos.* **124** 6222–37
[49] Horel J D and Wallace J M 1981 Planetary-scale atmospheric phenomena associated with the southern oscillation *Mon. Weather Rev.* **109** 813–29
[50] Wallace J M and Gutzler D S 1981 Teleconnections in the geopotential height field during the northern hemisphere winter *Mon. Weather Rev.* **109** 784–812
[51] Wang C 2002 Atlantic climate variability and its associated atmospheric circulation cells *J. Clim.* **15** 1516–36
[52] Wu Z, Wang B, Li J and Jin -F-F 2009 An empirical seasonal prediction model of the east Asian summer monsoon using ENSO and NAO *J. Geophys. Res.: Atmos.* **114** D18120
[53] Laufkötter C, Zscheischler J and Frölicher T L 2020 High-impact marine heatwaves attributable to human-induced global warming *Science* **369** 1621–5
[54] Frölicher T L, Fischer E M and Gruber N 2018 Marine heatwaves under global warming *Nature* **560** 360–4